Impact of millimetric to micrometric inter-electrode distances: Is there a way to maximize the organic pollutant degradation yield and minimize the cathode scaling and chlorate formation during wastewater treatment?

Saad Diris, Faidzul Hakim Adnan, Marie-Noëlle Pons, Emmanuel Mousset

Impact of millimetric to micrometric inter-electrode distances: Is there a way to maximize the organic pollutant degradation yield and minimize the cathode scaling and chlorate formation during wastewater treatment?

Saad Diris[a], Faidzul Hakim Adnan[a,b], Marie-Noëlle Pons[a], Emmanuel Mousset[a,1,*]

[a] *Université de Lorraine, CNRS, LRGP, F-54000 Nancy, France*

[b] *Sustainable Process Engineering Centre (SPEC), Department of Chemical Engineering, Faculty of Engineering, Universiti Malaya, 50603 Kuala Lumpur, Malaysia*

[1] *Present address: Nantes Université, ONIRIS, CNRS, GEPEA, UMR 6144, F-85000 La Roche-sur-Yon, France*

ACCEPTED IN

Electrochimica Acta

SI from ISE annual meeting 2023 – Symposium 10

*Contact of corresponding author: emmanuel.mousset@cnrs.fr

HIGHLIGHTS

- No compensation of anodic H^+ with cathodic OH^- at 50 µm at sufficiently high current
- Short distance (50 µm) could lead to high degradation yield with higher current
- With 50 µm, it still required higher energy to reach similar degradation efficiency
- A distance of 500 µm led to higher degradation, lower scaling and chlorate formation

ABSTRACT

The influence of a range of inter-electrode distances from 50 µm to 1 mm has been investigated for the first time, in order to assess to possibility to maximize the degradation and mineralization efficiency, while minimizing the cathode scaling and the inorganic by-products formation. Tylosin has been selected as representative pharmaceutical pollutant in wastewater, while the influence of Ca^{2+}, HCO_3^-/CO_3^{2-} and Cl^- was carried out. Advanced electro-oxidation with boron-doped diamond (BDD) anode and stainless-steel cathode was implemented to treat this synthetic effluent in a scalable filter-press reactor operated in a recirculated batch flow-by mode.

The first interesting feature is that cathodic OH^- and anodic H^+ formations were not counterbalanced at short micro-distances (50 µm), meaning that electro-precipitation (until 50% of $CaCO_3$ precipitation) and degradation/mineralization (until 100%) could still occur at such range of distance. Secondly, the gain of mass transfer at the shorter distance (50 µm) couldn't counteract the higher energy needed to achieve similar degradation efficiency compared to the distances of 500 µm and 1 mm. Lastly, too high distances such as 1 mm suffer from lower mass transfer compared to sub-millimetric distances. Thus, an intermediate distance of 500 µm led to better performance in terms of tylosin degradation (100% of degradation, 39% of mineralization), while minimizing electro-precipitation (26% of $CaCO_3$ cathodic precipitation) and unwanted inorganic chlorinated by-products formation (ClO_3^- = 2.8 mg L^{-1}). This was obtained at a current density of 0.1 mA cm^{-2}, leading to lower energy requirement (0.018 kWh g-tylosin^{-1}). In these low-current conditions the formation of perchlorate could be avoided.

Keywords:

Chlorinated by-products, anodic oxidation, electro-precipitation, microfluidic, pharmaceuticals

1. Introduction

Industrial processes generate enormous quantities of hazardous effluents every day, consisting of a very complex mixture of different organic and inorganic compounds and some of them can be toxic and difficult to degrade [1,2]. In addition, most of current urban wastewater treatment plants (WWTPs) are releasing emerging pollutants (e.g. pharmaceuticals, cosmetics, pesticides, etc) that are potentially toxic at even trace levels [3,4]. WWTPs are mainly implementing biological processes, which are not sufficient to remove completely these biorecalcitrant pollutants [3,5].

Therefore, it is necessary to implement innovative and more sustainable technologies able to deal with complex matrices in order to remove recalcitrant organic contaminants [6–8]. Among them, separation technologies have been proposed (e.g. adsorption, membrane filtration), but they only transfer the pollutants from one matrix to another one, while there is the need to deal with concentrates, altered membranes and saturated adsorbents [5,9]. Contrastingly, conversion processes allow eliminating the emerging contaminants, and particularly the advanced oxidation processes (AOPs) that can be implemented in mild conditions compared to thermal technologies for instance. This is due to the formation of highly oxidative compounds such as hydroxyl radicals ($^{\bullet}$OH), which is possible at ambient pressure and temperature [10]. Among AOPs, electrochemical advanced oxidation processes (EAOPs), such as advanced electro-oxidation, benefit from advantages of low footprint and high treatment efficiency with the continuous *in situ* production of oxidants, the latter depending on the nature of the anode used [11–15]. To promote water oxidation and the formation of $^{\bullet}$OH, boron-doped diamond (BDD) is often used as an anode. Its electrochemical properties give a high oxygen evolution overvoltage (2.4-2.6 V/Standard hydrogen electrode (SHE)), which allows the generation of these powerful oxidants [16–18].

Still, there are drawbacks of electrolytic treatments, such as the possible formation of by-products that are more toxic than the original compounds such as chlorine oxyanions (i.e., chlorate (ClO_3^-), perchlorate (ClO_4^-)) in the presence of inorganic ions [19–23]. This is well-known to occur at sufficiently high applied current density, at which the electrode potential is high enough to form ClO_3^-, and higher enough then to form ClO_4^- [19–23].

An additional disadvantage is that during the electrolytic process, electro-precipitation occurs in parallel on the surface of the cathode, in the presence of water containing Ca^{2+} and HCO_3^- /CO_3^{2-} ions (Eq. 1) [24–30].

$$Ca^{2+} + CO_3^{2-} \rightarrow CaCO_3 \quad (1)$$

This is due to the local alkalization at the vicinity of the cathode surface through H_2O (Eq. 2) and O_2 (Eq. 3) reduction reactions [31–34].

$$2H_2O + 2e^- \rightarrow H_2 + 2OH^- \quad (2)$$

$$O_2 + 2H_2O + 4e^- \rightarrow 4OH^- \quad (3)$$

Technical and economic issues related to the formation of limescale in industrial installations and domestic equipment have triggered research on this subject for a long time. The polarity reversal technique between the cathode and the anode has been identified as a solution applicable on an industrial scale, but still requires that the cathode material withstand high anodic potentials [35]. This ends up with the need to use more expensive and less sustainable cathode materials that involve more noble metals. The inter-electrode distance (d_{elec}) has shown recently having an impact on the cathodic electro-precipitation yield [33]. When short micro-distance (50 µm) was applied, it was remarkably noticed the absence of electro-precipitation at a given applied current density (j_{app}) (4 mA cm^{-2}) [33]. One of the hypotheses made was that

there could be a pH counterbalance between the cathodic accumulation of OH^- with the anodic generation of H^+ (Eq. 4) in the thin film undivided cell, leading to the absence of cathodic alkalization [33].

$$2H_2O \rightarrow O_2 + 4H^+ + 4e^- \quad (4)$$

However, this assumption remains to be tested at higher applied current. Moreover, the efficiency of degradation has to be verified at such higher range, i.e. in the range where the anodic potential is sufficiently high to produce •OH.

Existing papers on the topic propose the optimization of electrochemical processes by considering the degradation/mineralization efficiency and in a lesser extend the formation of unwanted by-products [15,36–38]. However, to the best of authors' knowledge, the literature never took into account the possibility of electro-precipitation as additional criterion of efficiency, though precipitating ions are frequently detected in effluents.

In this context, this paper aims to evaluate for the first time the operating conditions for which there would be maximum degradation and mineralization of organic pollutants, while having minimal $CaCO_3$ electro-precipitation and minimal formation of chlorate and perchlorate. The electro-oxidation process was applied in a scalable filter-press type electrochemical reactor in order to extrapolate more easily the results at industrial scale. Micrometric to millimetric d_{elec} (50-1000 µm) were considered to check the hypothesis above-mentioned that could occur at the shortest distance (i.e., 50 µm). J_{app} was varied for each d_{elec} in order to assess the efficiency of degradation and mineralization of tylosin as representative organic pharmaceutical pollutant in wastewater, in the presence or absence of chloride ions that are also frequently found in wastewaters [39]. Preferentially low J_{app} were tested in order to minimize the potential production of chlorine oxyanions.

2. Experimental

2.1. Preparation of the synthetic effluent

The synthetic effluents were prepared in 5 L of ultrapure water at 18.2 MΩ.cm (PureLab ELGA Classic, Veolia Water, Antony, France), by adding 150 mg L^{-1} of $CaSO_4.2H_2O$ (VWR International, Fontenay-sous-Bois, France), 60 mg-C L^{-1} of $NaHCO_3$ (VWR International, Fontenay-sous-Bois, France), 1.625 mL of H_2SO_4 (1 M) (Sigma Aldrich, Saint-Quentin-Fallavier, France) to adjust the pH to a neutral value. Tylosin tartrate (10 mg L^{-1}) (Sigma Aldrich, Saint-Quentin-Fallavier, France) was added to all effluents as representative biorecalcitrant pollutant to study the degradation and mineralization efficiency of the advanced electro-oxidation process in the presence of electro-precipitation. The effect of the presence of Cl^- ions (130 mg L^{-1}) was carried out by adding NaCl (3 mM) and KCl (0.43 mM) (Techlab, Metz, France). All reagents were of analytical grade.

2.2. Electrochemical setup

An electrochemical filter-press cell composed of two parallel plates placed vertically was used with BDD doped on Niobium plate (50 cm^2 of active geometric surface) (DiaCCon, Fürth, Germany) as anode and 316L stainless steel plate (50 cm^2 of active geometric surface) (Gantois Industries, Saint-Dié-des-Vosges, France) as cathode as previously described [26,40]. For all experiments, 500 mL of synthetic effluent was treated in batch recirculated mode using a peristaltic pump (Masterflex, Cole Parmer). The flow rates were varied from 10 to 100 and 200 mL min^{-1} with increasing d_{elec} (50, 500 and 1000 µm, respectively) using polytetrafluoroethylene (PTFE) spacer (Bohlender, Grünsfeld, Germany), in order to obtain the same residence time within the electrolyzer [33]. The electrolysis was carried out using a

current generator (HAMEG, Rohde & Schwarz, Meudon-la-Forêt, France), by varying the current density from 0.02 to 20 mA cm^{-2} (1 to 1000 mA). After each electrolysis, the cathode was immersed in 300 mL of a sulfuric acid solution (0.25 M) for 24 h to redissolve the electro-precipitate and measure the amount of calcium (Ca) [26].

2.3. Analytical methods

The analyzes of total inorganic carbon (TIC) and total organic carbon (TOC) were carried out with a Shimadzu V_{CSH} type TOC meter (Marne-La-Vallée, France). The samples were filtered to 0.45 µm to get the dissolved organic fraction. TOC was determined using the non-purgeable organic carbon (NPOC) method. TIC values allow monitoring the content of carbonates and bicarbonates in solution.

The calcium concentration was monitored with inductively coupled plasma - optical emission spectroscopy (ICP-OES) of the Thermo iCAP 6000 type (Thermo Fisher, Noisy-le-Grand, France). The collected samples (0.5 mL) were filtered with Phenex™ (Phenomenex, Le Pecq, France) 0.45 µm syringe filter and were dissolved with 4.5 mL of H_2SO_4 (0.5 M). Standard Ca^{2+} solutions were prepared from 1 to 20 mg L^{-1} to establish the calibration curve using a certified multi-element solution at 1000 mg L^{-1} (SCP Sciences, Villebon-sur-Yvette, France). The calcium element concentration quantified in solution was assimilated to ionic calcium (Ca^{2+}) concentration [26].

High-performance liquid chromatography (HPLC) was used to identify and quantify tylosin molecule. The samples were previously filtered at 0.45 µm (Phenex™). The HPLC was composed of a pump, a column oven, a column (Kinetex® reversed phase C18; 2.6 µm average particle size, 4.6 mm internal diameter, 100 mm length) (Phenomenex, Le Pecq, France) and a photodiode array detector (maximal absorbance of tylosin at 290 nm). The pump operated in

isocratic mode with a solvent composed of acetonitrile (65%) and ultrapure water including 1% formic acid (35%), with a flow rate of 0.6 mL min^{-1}, an injection volume of 50 µL and a temperature of 25°C.

The concentrations of Cl^-, ClO_3^- and ClO_4^- ions were quantified by ionic chromatography (IC) using the Dionex™ ICS-6000 Capillary HPIC™ equipment (Thermo Scientific, Noisy-Le-Grand, France) following a previous method [20]. The ion separation and quantification were done using the AS19 IC Dionex™ IonPac™ analytical column (Thermo Scientific, Noisy-Le-Grand, France). It allows obtaining the speciation of chlorine oxyanions. The samples were filtered at 0.45 µm (Phenex™) and analyzed without previous dilution.

The anodic potentials were obtained by chronopotentiometry method, as well as cyclic voltammetry, using a potentiostat (Ametek, Massy, France) connected to the setup described in section 2.2 and elsewhere [40], using a saturated silver chloride reference electrode.

2.4. Performance parameters

The degradation yield of tylosin was defined as follow (Eq. 5):

$$Degradation\ yield\ (\%) = 1 - \frac{[Tyl]}{[Tyl]_0} \quad (5)$$

where [Tyl] and $[Tyl]_0$ are the concentrations (mg L^{-1}) of tylosin at time *t* and at *t* = 0 (initial).

The mineralization yield was considered as follow (Eq. 6):

$$Mineralization\ yield\ (\%) = 1 - \frac{TOC}{TOC_0} \quad (6)$$

where TOC and TOC_0 are the TOC concentrations (mg-C L^{-1}) at time *t* and at *t* = 0 (initial).

The electro-precipitation yield was expressed as follow (Eq. 7):

$$Electro - precipitation\ yield\ (\%) = 1 - \frac{[Ca^{2+}]}{[Ca^{2+}]_0} \quad (7)$$

where $[Ca^{2+}]$ and $[Ca^{2+}]_0$ are the concentrations (mg L^{-1}) of calcium at time t and at $t = 0$ (initial).

The specific energy consumption (E_{sp}), expressed in kWh g-tylosin^{-1}, was defined as follow (Eq. 8) [41]:

$$E_{sp} = \frac{U \times I \times t}{V \times ([Tyl]_t - [Tyl]_0)} \quad (8)$$

where U is the cell voltage (V), I is the applied current intensity (A), t is the electrolysis time (h), V is the solution volume (L).

3. Results and discussion

3.1. Influence of j_{app} and d_{elec} on electro-oxidation

The results obtained for the tests carried out at different current intensities (1 to 1000 mA) and distances (50, 500, 1000 µm) after 5 h of electrolysis are presented in Figure 1. The tylosin degradation results are taken from the kinetics shown in Figure S1.

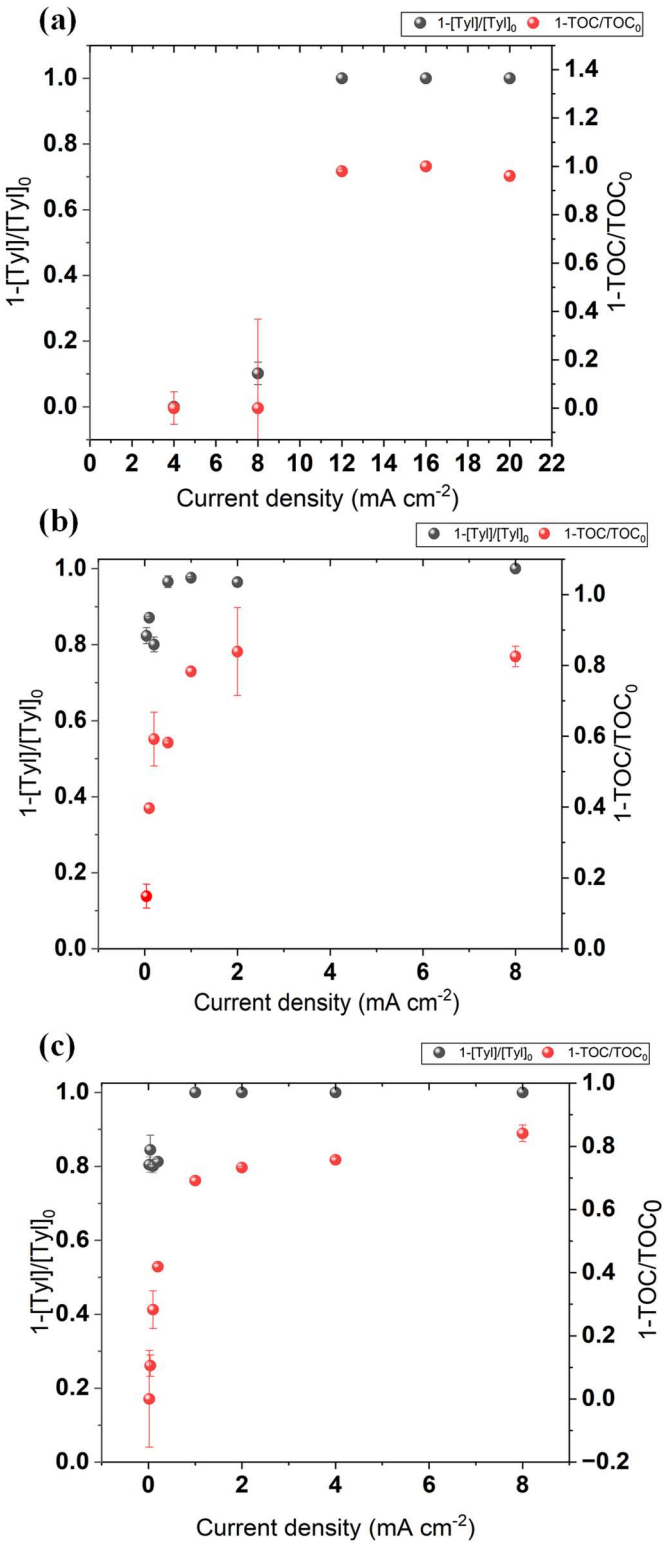

Figure 1. Evolutions of tylosin and TOC as a function of j_{app} after 5 h of electrolysis and at different d_{elec}: (a) 50 µm, (b) 500 µm, (c) 1000 µm. Operating conditions: anode: BDD; cathode: stainless steel; $[tyl]_0$ = 10 mg L^{-1}; $[CaSO_4.2H_2O]$ = 150 mg L^{-1}; $[NaHCO_3]$ = 60 mg-C L^{-1}.

TOC results indicated that increasing j_{app} for all three d_{elec} resulted in increased degradation and mineralization rates until reaching a plateau. For 50 µm, the maximum mineralization (around 100%) was reached after 4 h of electrolysis with a j_{app} of 16 mA cm^{-2} (1.6 Ah L^{-1}) (Figure 1a). For 500 µm, the mineralization rate increased from 14% (0.04 mA cm^{-2}) to 83% (8 mA cm^{-2}) (Figure 1b). This maximum is reached after 5 h of treatment, for a j_{app} of 2 mA cm^{-2} (0.25 Ah L^{-1}). A similar mineralization rate (84%) is obtained for a j_{app} of 8 mA cm^{-2} (1 Ah L^{-1}) at 1000 µm after 5 h (Figure 1c). Concerning the complete degradation of tylosin, it is reached at a j_{app} of 12 mA cm^{-2} (0.8 Ah L^{-1}) for 50 µm, 8 mA cm^{-2} (0.8 Ah L^{-1}) for 500 µm, and 1 mA cm^{-2} (0.1 Ah L^{-1}) for 1000 µm.

The trends observed at a given d_{elec} can be explained by the fact that •OH production increased with j_{app}, and therefore increased the kinetics of tylosin degradation (Figure S1) and mineralization. In addition, E_{sp} decreased with the decrease of d_{elec}, except for 50 µm (Figure S2). Table 1 shows the values of E_{sp} for each distance after 5 h of electrolysis. Considering all these parameters, the conditions which allow total degradation of tylosin, relatively significant mineralization, while minimizing energy consumption, are a distance of 500 µm with a j_{app} of 8 mA cm^{-2}.

Table 1. Values of E_{sp} consumed for each distance at maximal degradation yield (100%) and mineralization yield, i.e., after 5 h of electrolysis.

d_{elec} (µm)	Mineralization yield (%)	Degradation yield (%)	j_{app} (mA cm^{-2})	E_{sp} (kWh g-tylosin^{-1})
50	~ 100	~ 100	12	2.76
500	83	~ 100	8	1.84
1000	84	~ 100	8	2.26

3.2. Influence of j_{app} and d_{elec} on cathodic electro-precipitation

The calcium elimination yields after 5 h of electrolysis as well as the kinetics of Ca and TIC obtained for the tests carried out at different j_{app} (0.02 to 20 mA cm^{-2}) and various d_{elec} (50, 500 and 1000 µm) are shown in Figure 2, Figure S3 and Figure S4, respectively. The evolutions of Ca and TIC followed the same trend for the three d_{elec}. Cathodic electro-precipitation increased with j_{app}, then reached a maximum, and finally a decrease in precipitation was observed from a certain j_{app}. This drop is linked to the significant production of H_2 bubbles on the surface of the cathode at high j_{app}, as suggested by a previous study [33].

Furthermore, the increase in j_{app} for the three d_{elec} resulted from an increase in Ca precipitation and $CaCO_3$ formation from 0% to 50% by varying the intensities from 200 to 1000 mA at a distance of 50 µm. The maximum precipitation (50%) was obtained after 5 h for a density of 16 mA cm^{-2} (2 Ah L^{-1}), then decreased to 40% for a density of 20 mA cm^{-2} (2.5 Ah L^{-1}). At a distance of 500 µm, electro-precipitation increased by 12 to 65% over a current density range of 0.04 to 8 mA cm^{-2}. The maximum precipitation (65%) was reached after 5 h with a j_{app} of 1 mA cm^{-2} (0.125 Ah L^{-1}), then we notice a reduction in the formation of $CaCO_3$ to 61 and 41% for 2 and 8 mA cm^{-2} respectively. For the distance of 1000 µm, the electro-precipitation increased from 4 to 68% by increasing j_{app} from 0.02 to 8 mA cm^{-2}, reaching the maximum (68%) with a density of 1 mA cm^{-2} (0.125 Ah L^{-1}). Beyond this current, a decrease in electro-precipitation to 57% and 32% was observed, for 2 and 4 mA cm^{-2}, respectively.

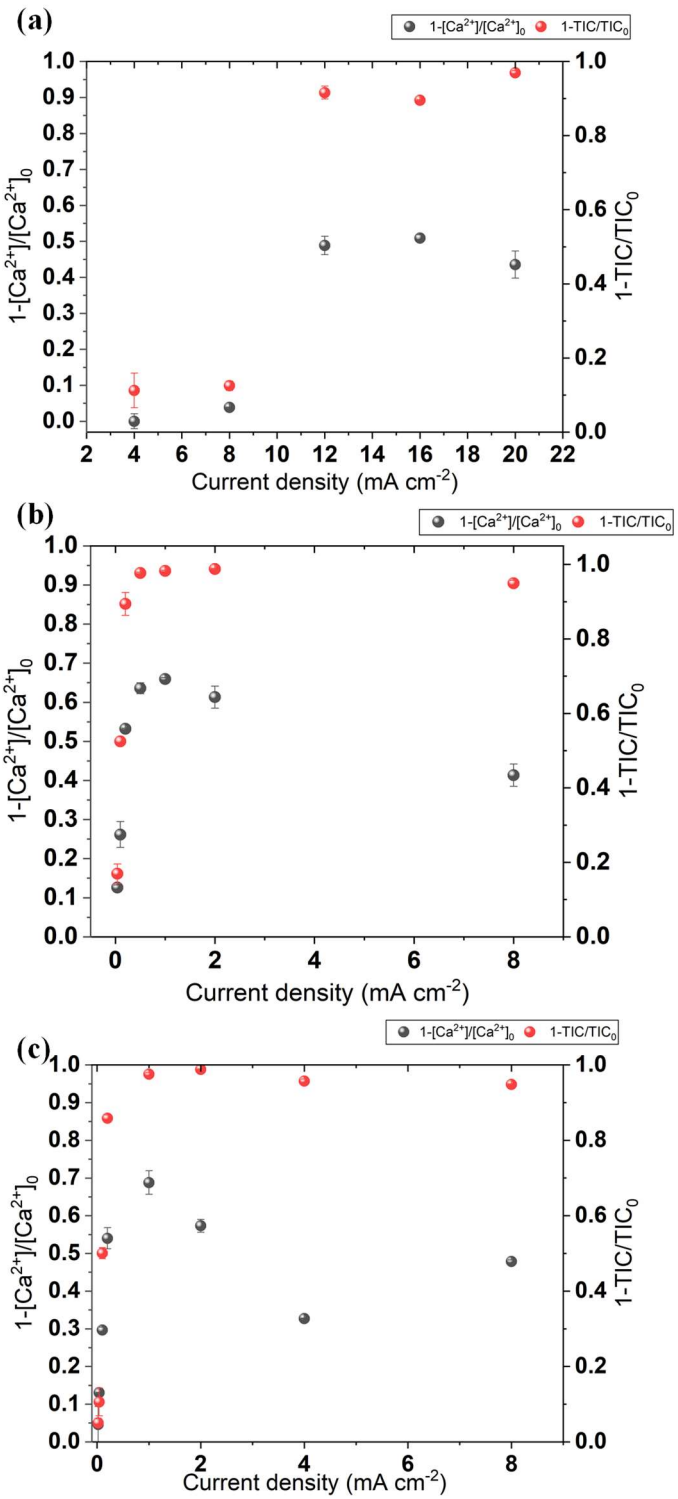

Figure 2. Evolutions of Ca^{2+} and CIT as a function of j_{app} after 5 h of electrolysis and at different d_{elec}: (a) 50 µm, (b) 500 µm, (c) 1000 µm. Operating conditions: anode: BDD; cathode: stainless steel; $[tyl]_0$ = 10 mg L^{-1}; $[CaSO_4.2H_2O]$ = 150 mg L^{-1}; $[NaHCO_3]$ = 60 mg-C L^{-1}.

The changes in the bulk pH and the ionic conductivity throughout the electrolysis were monitored to complete the study (Figure S5). The first observation is that the conductivity and the pH tended to decrease during the electro-precipitation process. This decrease in the solution pH was attributed to the modification of the thermodynamic equilibrium of HCO_3^-/CO_3^{2-} in favor to the formation of CO_3^{2-} by reacting with OH^- (Eq. 9), which led to the accumulation in the bulk of H^+ generated at the anode (Eq. 4) [26].

$$OH^- + HCO_3^- \rightarrow H_2O + CO_3^{2-} \quad (9)$$

The only case where the pH did not decrease corresponded to electrolysis with low j_{app}, that is to say when the electro-precipitation process was weak. The decrease in ionic conductivity can be interpreted by the consumption of OH^- and CO_3^{2-} during electro-precipitation.

Taking into account all these factors, it was possible to minimize electro-precipitation at a d_{elec} of 50 µm and j_{app} equaled to 4 mA cm^{-2} (200 mA). However, at this distance and at this current the degradation is negligible (Figure 1a). Thus, with low d_{elec}, higher densities must be applied than at larger d_{elec}, to obtain sufficient anode potential to degrade organic compounds. This implies greater energy consumption, as mentioned in section 3.1.

3.3. Conditions for a high degradation yield and a minimized precipitation

The main practical objective of this study was to assess the possibility to degrade organic pollutants, while minimizing electro-precipitation to avoid the scaling constraints and associated polarity reversal. Figure 3 illustrates the evolution of calcium and tylosin for different d_{elec} and at j_{app} which led to a better compromise between the tylosin degradation and electro-precipitation (12 mA cm^{-2} for 50 µm and 0.1 mA cm^{-2} for 500 and 1000 µm). It is noticed that with a d_{elec} of 50 µm, the organic pollutant was completely degraded but at the

same time there was 48% of electro-precipitation on the cathode surface. On the other hand, for the other distances (500 and 1000 µm) there was a significant degradation of tylosin (87% and 80% for 500 and 1000 µm respectively), for a precipitation of 26% and 29% of $CaCO_3$ at 500 and 1000 µm respectively.

It could be further noted that even at low current for 500 and 1000 µm (5 mA, 0.1 mA cm^{-2}), the tylosin degradation was still very high. At such current, the anodic potentials were 2.0 and 2.4 V/SHE with 500 µm and 1000 µm, respectively. These potentials are too low to generate physisorbed •OH at the BDD surface. Moreover, it was noticed a plateau of apparent rate constants (k_{app}) (assuming pseudo-first order kinetic model) of tylosin degradation at 500 µm and 1000 µm for low j_{app} (0.02 – 0.2 mA cm^{-2}), while k_{app} values are increasing at higher j_{app} (Figure S6). This trend is corroborating the fact that direct oxidation of tylosin should occur at low j_{app}. Moreover, cyclic voltammetry study have shown a peak at around 1.7 V vs Ag/AgCl, which could be related to the direct oxidation of tylosin as •OH are not formed at such potential (Figure S7). This was in agreement with a previous article that highlighted the electroactivity of tylosin through a more pronounced peak using a nickel electrode in basic aqueous solution and in absence of O_2 (i.e., under N_2 atmosphere) [42]. Therefore, the possibility of degrading tylosin at such low j_{app} should be induced by the fact that tylosin is an electroactive species that can react by direct oxidation at the anode.

Thus, a distance of 500 µm appeared to give better performance (j_{app} = 0.1 mA cm^{-2} (5 mA), E_{sp} = 0.018 kWh g-tylosin^{-1}) than 1000 µm, while 50 µm led to 153-times higher energy requirement in order to get sufficient degradation yield (Table 2). It is already known that a distance of 500 µm involved higher mass transport coefficient than millimetric ones [40], while such range of distances allows operating with low-conductivity solution and decreasing the ohmic drop and therefore the energy consumption [43–46]. However, this paper highlights that too low distance (i.e., 50 µm) that involve even higher mass transport, do not compensate the

need to increase the current density to lead to similar degradation efficiency compared to higher distances.

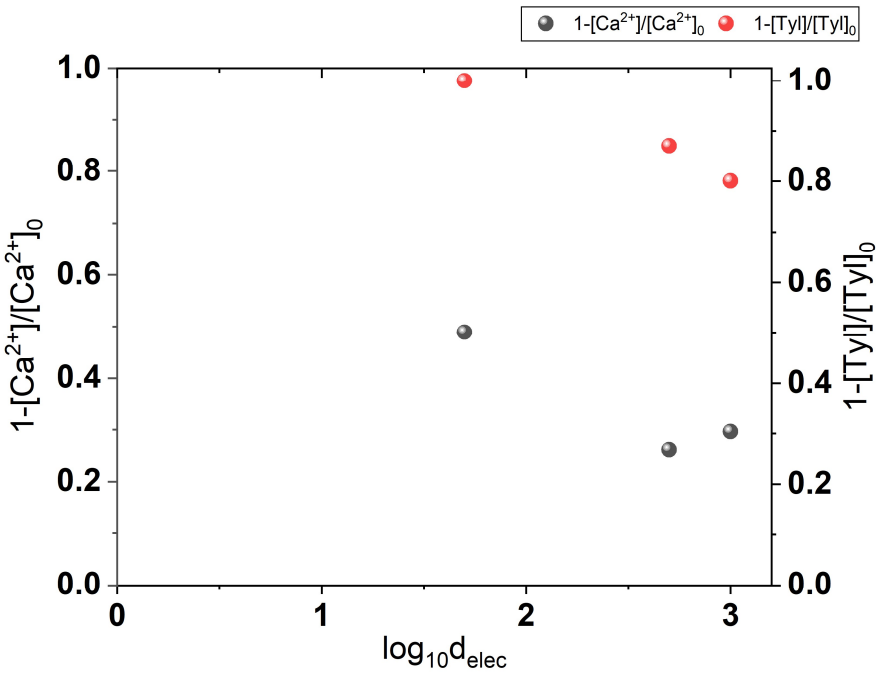

Figure 3. Evolutions of Ca^{2+} and tylosin after 5 h of electrolysis at different d_{elec}. Operating conditions: anode: BDD; cathode: stainless steel; I = 600 mA for 50 µm; I = 5 mA for 500 and 100 µm; $[tyl]_0$ = 10 mg L^{-1}; $[CaSO_4.2H_2O]$ = 150 mg L^{-1}; $[NaHCO_3]$ = 60 mg-C L^{-1}.

Table 2. Values of E_{sp} consumed for each distance at minimal electro-precipitation yield and at maximal degradation and mineralization yield.

d_{elec} (µm)	Mineralization yield (%)	Degradation yield (%)	Electro-precipitation yield (%)	j_{app} (mA cm^{-2})	E_{sp} (kWh g-tylosin^{-1})
50	97	100	48	12	2.76
500	39	87	26	0.1	0.018
1000	28	80	28	0.1	0.019

3.4. Influence of chloride ions

Cl^- ions are often present in wastewater and are easily oxidized under advanced electro-oxidation conditions [47]. In particular, they can interfere with •OH and generate potentially toxic by-products. Therefore, it seemed important to study the influence of the presence of chlorides in solutions which already contain Ca^{2+}, HCO_3^- and tylosin for different d_{elec} (Figure 4). This has been carried out with distances of 500 µm and 1 mm, because studies with 50 µm depicted too high energy-intensive condition in Section 3.3 and this is not suitable for industrial applications. The experiments have been performed at a j_{app} equaled to 0.1 mA cm^{-2} as it has been assumed from previous Section 3.3 to be a good compromise between the degradation and the electro-precipitation yields. This condition could also limit the production of chlorine oxyanions, which is studied in this Section 3.4. Figure 4 shows that the chloride concentration decreases very slightly during electrolysis regardless of the d_{elec} applied (500 and 1000 µm), which indicates that the electro-oxidation was sufficiently weak for the Cl^- to ultimately poorly react. However, chromatographic analyzes showed the presence of chlorates, the concentration of which increased slightly and gradually during the treatments, for the two d_{elec} tested. These chlorinated by-products have a toxic effect on human health [48]. It is therefore important to minimize their formation while maximizing tylosin degradation. It was also noted that with 1000 µm the formation of chlorates was faster than with 500 µm. This can be justified by the increase in the d_{elec} which leads to the increase in the voltage across the electrochemical cell.

The slight decrease in Cl^- concentrations could be explained by the low formation of chlorates in parallel. Indeed, the oxidation of Cl^- at the anode can lead to the formation of Cl_2 (Eq. 10), then Cl_2 to HClO (Eq. 11), HClO to ClO_2^- (Eq. 12), and finally ClO_2^- to ClO_3^- (Eq. 13), as suggested in the literature [20,48].

$$2Cl^- \rightarrow Cl_2(g) + 2e^- \quad (10)$$

$$Cl_2(g) + H_2O \rightarrow HClO + H^+ + Cl^- \quad (11)$$

$$HClO + {}^{\bullet}OH \rightarrow ClO_2^- + 2H^+ + e^- \quad (12)$$

$$HClO + ClO_2^- \rightarrow ClO_3^- + H^+ + Cl^- \quad (13)$$

The accumulation and lifespan of HClO and ClO_2^- is low compared to that of ClO_3^- which is stable. It is also important to notice that with the low applied currents (5 mA), there was no production of perchlorate (ClO_4^-), since the oxidation conditions are not strong enough.

Thus, applying a j_{app} of 0.1 mA cm^{-2} for d_{elec} of 500 and 1000 µm seems to be interesting for both degrading tylosin and mineralizing the solution while minimizing electro-precipitation and the formation of chlorinated by-products.

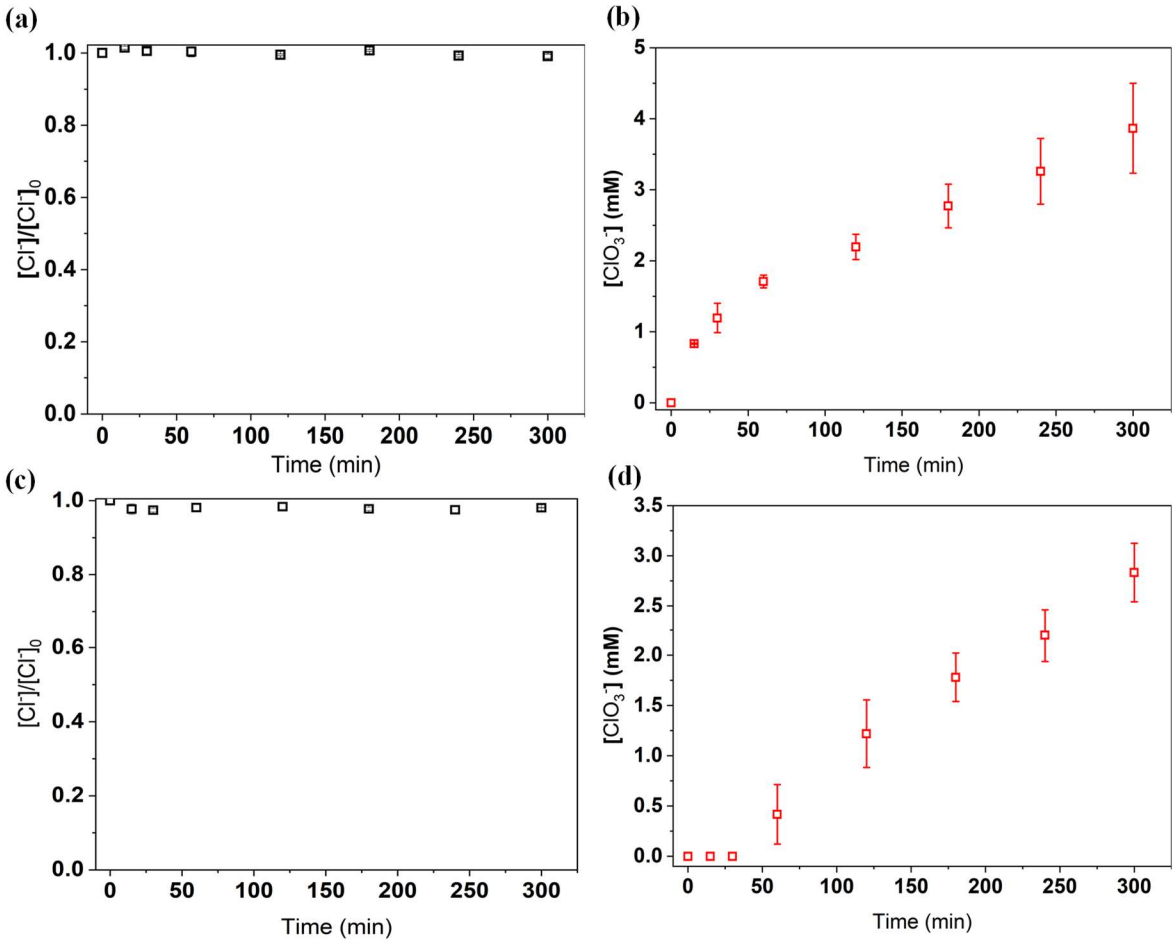

Figure 4. Evolutions of Cl^- and ClO_3^- concentrations as a function of time and at different d_{elec}: (a, b): 1000 µm, (c, d): 500 µm. Operating conditions: anode: BDD; cathode: stainless steel; I = 5 mA; $[tyl]_0$ = 10 mg L^{-1}; $[CaSO_4.2H_2O]$ = 150 mg L^{-1}; $[NaHCO_3]$ = 60 mg-C L^{-1}; $[Cl^-]$ = 130 mg L^{-1}.

4. Conclusions

The main objective of this work was to investigate the possibility of degrading organic pollutants, tylosin as the representative compound in this study, while minimizing electro-precipitation on the cathode surface and limiting the formation of potentially toxic inorganic by-products in the presence of chlorides. Three d_{elec} (50, 500 and 1000 µm) were tested in a filter-press type reactor, including micro-distances for their interest in applications with poorly conductive effluents as well as for the intensification of transfers. The current was varied for each distance (from 1 to 1000 mA), which corresponded to j_{app} values between 0.02 and 20 mA cm^{-2}.

For each distance, the conditions which make it possible to obtain degradation of tylosin and mineralization while reducing electro-precipitation and the quantity of ClO_3^- formed are as follows (after 5 h of electrolysis):

- At 50 µm: 12 mA cm^{-2} (600 mA; 1.5 Ah L^{-1}) for a degradation rate of 100% (2.76 kWh g-$tylosin^{-1}$), mineralization of 97% and $CaCO_3$ electro-precipitation of 48%

- At 500 µm: 0.1 mA cm^{-2} (5 mA; 0.0125 Ah L^{-1}) for a degradation rate of 87% (0.018 kWh g-$tylosin^{-1}$), mineralization of 39%, $CaCO_3$ electro-precipitation of 26%, and giving rise to a ClO_3^- concentration of 2.8 mg L^{-1}

- At 1000 µm: 0.1 mA cm^{-2} (5 mA; 0.0125 Ah L^{-1}) for a degradation rate of 80% (0.019 kWh g-$tylosin^{-1}$), mineralization of 28%, $CaCO_3$ electro-precipitation of 29%, and giving rise to a ClO_3^- concentration of 3.9 mg L^{-1}

It is interesting to point out that even at a short micro-distance (50 µm), electro-precipitation took place, as well as the degradation and mineralization of the solution could occur in parallel. This means that by applying sufficiently high current density, faradaic reactions could still take

place. This also means that the hypothesis of the compensation of the H^+ produced at the anode with the OH^- generated at the cathode, which could avoid electro-precipitation at such low micro-distances (50 µm), is ultimately not valid. This further means that at such low distance, there is the need to increase the current density to get similar degradation efficiency compared to higher distances (i.e., 500 and 1000 µm), which increase drastically the energy requirement then (153-times higher than at 500 and 1000 µm).

It is also important to note that the conditions obtained are valid with tylosin which finally appears to be electroactive, which implies that it can be electro-oxidized by direct contact with the anode without the need to apply very high current densities. As one of the perspectives, it could be interesting to compare these trends with a non-electroactive organic pollutant, in terms of optimal conditions required.

Acknowledgments

This work has been supported by the French National Research Agency through the REMixSyn project (n°ANR-21-CE04-0006-01).

References

[1] O. Garcia-Rodriguez, E. Mousset, H. Olvera-Vargas, O. Lefebvre, Electrochemical treatment of highly concentrated wastewater: A review of experimental and modeling approaches from lab- to full-scale, Crit Rev Environ Sci Technol 52 (2022) 240–309. https://doi.org/10.1080/10643389.2020.1820428.

[2] F.C. Moreira, R.A.R. Boaventura, E. Brillas, V.J.P. Vilar, Electrochemical advanced oxidation processes: A review on their application to synthetic and real wastewaters, Appl Catal B 202 (2017) 217–261. https://doi.org/10.1016/j.apcatb.2016.08.037.

[3] J. Margot, L. Rossi, D.A. Barry, C. Holliger, A review of the fate of micropollutants in wastewater treatment plants, Wiley Interdisciplinary Reviews: Water 2 (2015) 457–487. https://doi.org/10.1002/WAT2.1090.

[4] S.D. Richardson, S.Y. Kimura, Water Analysis: Emerging Contaminants and Current Issues, Anal Chem 88 (2016) 546–582. https://doi.org/10.1021/acs.analchem.5b04493.

[5] S. Besnault, S. Martin, S. Baig, H. Budzinski, K. Le Menach, M. Esperanza, N. Noyon, C. Gogot, C. Miège, L. Dherret, A. Roussel-Galle, M. Coquery, Réduction des micropolluants par les traitements complémentaires : procédés d'oxydation avancée, adsorption sur charbon actif (ARMISTIQ – Action A), 2014.

[6] L. Rizzo, W. Gernjak, P. Krzeminski, S. Malato, C.S. McArdell, J.A.S. Perez, H. Schaar, D. Fatta-Kassinos, Best available technologies and treatment trains to address current challenges in urban wastewater reuse for irrigation of crops in EU countries, Science of the Total Environment 710 (2020) 136312. https://doi.org/10.1016/j.scitotenv.2019.136312.

[7] E. Mousset, T.A. Hatton, Advanced hybrid electro-separation/electro-conversion systems for wastewater treatment, reuse and recovery: compromise between symmetric and asymmetric constraints, Curr Opin Electrochem 35 (2022) 101105. https://doi.org/10.1016/j.coelec.2022.101105.

[8] E. Mousset, M. Fournier, X. Su, Recent advances of reactive electroseparation systems for water treatment and selective resource recovery, Curr Opin Electrochem 42 (2023) 101384.

[9] S. Besnault, S. Martin, Etat de l'art sur les procédés avancés intensifs pour la réduction de micropolluants dans les eaux usées traitées. Rapport bibliographique., 2011. http://www.onema.fr/IMG/pdf/valo/Livrable_2010_Action28-5_ARMISTIQ_ActionA_tertiairesintensifs_Vfin.pdf.

[10] M.A. Oturan, J.-J. Aaron, Advanced Oxidation Processes in Water/Wastewater Treatment: Principles and Applications. A Review, Crit Rev Environ Sci Technol 44 (2014) 2577–2641. https://doi.org/10.1080/10643389.2013.829765.

[11] M. Panizza, G. Cerisola, Direct and mediated anodic oxidation of organic pollutants, Chem Rev 109 (2009) 6541–6569. https://doi.org/10.1021/cr9001319.

[12] C.A. Martínez-Huitle, M. Panizza, Electrochemical oxidation of organic pollutants for wastewater treatment, Curr Opin Electrochem 11 (2018) 62–71. https://doi.org/10.1016/j.coelec.2018.07.010.

[13] E. Mousset, Interest of micro-reactors for the implementation of advanced electrocatalytic oxidation with boron-doped diamond anode for wastewater treatment, Curr Opin Electrochem 32 (2022) 100897. https://doi.org/10.1016/j.coelec.2021.100897.

[14] C.A. Martínez-Huitle, M.A. Rodrigo, I. Sirés, O. Scialdone, Single and coupled electrochemical processes and reactors for the abatement of organic water pollutants : A critical review, Chem Rev 115 (2015) 13362–13407. https://doi.org/10.1021/acs.chemrev.5b00361.

[15] C.A. Martínez-Huitle, M.A. Rodrigo, I. Sirés, O. Scialdone, A critical review on latest innovations and future challenges of electrochemical technology for the abatement of organics in water, Appl Catal B 328 (2023). https://doi.org/10.1016/j.apcatb.2023.122430.

[16] S.T. McBeath, D.P. Wilkinson, N.J.D. Graham, Application of boron-doped diamond electrodes for the anodic oxidation of pesticide micropollutants in a water treatment process: A critical review, Environ Sci (Camb) 5 (2019) 2090–2107. https://doi.org/10.1039/c9ew00589g.

[17] P. V. Nidheesh, G. Divyapriya, N. Oturan, C. Trellu, M.A. Oturan, Environmental applications of boron-doped diamond electrodes: 1. Applications in water and wastewater treatment, ChemElectroChem 6 (2019) 1–20. https://doi.org/10.1002/celc.201801876.

[18] E. Mousset, D.D. Dionysiou, Photoelectrochemical reactors for treatment of water and wastewater: a review, Environ Chem Lett 18 (2020) 1301–1318. https://doi.org/10.1007/s10311-020-01014-9.

[19] E. Mousset, S. Pontvianne, M.N. Pons, Fate of inorganic nitrogen species under homogeneous Fenton combined with electro-oxidation/reduction treatments in synthetic solutions and reclaimed municipal wastewater, Chemosphere 201 (2018) 6–12. https://doi.org/10.1016/j.chemosphere.2018.02.142.

[20] E. Mousset, L. Quackenbush, C. Schondek, A. Gerardin-Vergne, S. Pontvianne, S. Kmiotek, M.N. Pons, Effect of homogeneous Fenton combined with electron transfer on the fate of inorganic chlorinated species in synthetic and reclaimed municipal wastewater, Electrochim Acta 334 (2020) 135608. https://doi.org/10.1016/j.electacta.2019.135608.

[21] M.E.H. Bergmann, J. Rollin, T. Iourtchouk, The occurrence of perchlorate during drinking water electrolysis using BDD anodes, Electrochim Acta 54 (2009) 2102–2107. https://doi.org/10.1016/j.electacta.2008.09.040.

[22] M.E.H. Bergmann, A.S. Koparal, T. Iourtchouk, Electrochemical Advanced oxidation processes, formation of halogenate and perhalogenate species: A critical review, Crit Rev Environ Sci Technol 44 (2014) 348–390. https://doi.org/10.1080/10643389.2012.718948.

[23] a. Sánchez-Carretero, C. Sáez, P. Cañizares, M. a. Rodrigo, Electrochemical production of perchlorates using conductive diamond electrolyses, Chemical Engineering Journal 166 (2011) 710–714. https://doi.org/10.1016/j.cej.2010.11.037.

[24] F.H. Adnan, M. Pons, E. Mousset, Thin film microfluidic reactors in electrochemical advanced oxidation processes for wastewater treatment: A review on influencing parameters, scaling issues, and engineering considerations, Electrochemical Science Advances (2022). https://doi.org/10.1002/elsa.202100210.

[25] F.H. Adnan, S. Pontvianne, M.-N. Pons, E. Mousset, Roles of H2 evolution overpotential, materials porosity and cathode potential on mineral electro-precipitation in microfluidic reactor – New criterion to predict and assess interdependency, Electrochim Acta 428 (2022) 140926. https://doi.org/10.1016/j.electacta.2022.140926.

[26] F.H. Adnan, E. Mousset, S. Pontvianne, M.N. Pons, Mineral cathodic electro-precipitation and its kinetic modelling in thin-film microfluidic reactor during advanced electro-oxidation process, Electrochim Acta 387 (2021) 138487. https://doi.org/10.1016/j.electacta.2021.138487.

[27] F.H. Adnan, S. Pontvianne, M.-N. Pons, E. Mousset, Role of anodically electrogenerated hydroxyl radicals in minimizing mineral cathodic electroprecipitation in the presence of hard water, Electrochem Commun 150 (2023) 107493. https://doi.org/10.1016/j.elecom.2023.107493.

[28] Z. Belarbi, B. Sotta, L. Makhloufi, B. Tribollet, J. Gamby, Modelling of delay effect of calcium carbonate deposition kinetics on rotating disk electrode in the presence of green inhibitor, Electrochim Acta 189 (2016) 118–127. https://doi.org/10.1016/j.electacta.2015.12.089.

[29] Z. Belarbi, J. Gamby, L. Makhloufi, B. Tribollet, Nucleation-growth process of calcium carbonate on rotating disk electrode in mineral potable water, Electrochim Acta 109 (2013) 623–629. https://doi.org/10.1016/j.electacta.2013.07.148.

[30] Y. Ben Amor, L. Bousselmi, M.C. Bernard, B. Tribollet, Nucleation-growth process of calcium carbonate electrodeposition in artificial water-Influence of the sulfate ions, J Cryst Growth 320 (2011) 69–77. https://doi.org/10.1016/j.jcrysgro.2011.02.005.

[31] M.M. Tlili, M. Benamor, C. Gabrielli, H. Perrot, B. Tribollet, Influence of the Interfacial pH on Electrochemical CaCO[sub 3] Precipitation, J Electrochem Soc 150 (2003) C765. https://doi.org/10.1149/1.1613294/XML.

[32] Y. Lei, B. Song, R.D. Van Der Weijden, M. Saakes, C.J.N. Buisman, Electrochemical Induced Calcium Phosphate Precipitation: Importance of Local pH, Environ Sci Technol 51 (2017) 11156–11164. https://doi.org/10.1021/acs.est.7b03909.

[33] F.H. Adnan, S. Pontvianne, M.N. Pons, E. Mousset, Unprecedented roles of submillimetric interelectrode distances and electrogenerated gas bubbles on mineral cathodic electro-precipitation: Modeling and interface studies, Chemical Engineering Journal 431 (2022) 133413. https://doi.org/10.1016/j.cej.2021.133413.

[34] C. Deslouis, I. Frateur, G. Maurin, B. Tribollet, Interfacial pH measurement during the reduction of dissolved oxygen in a submerged impinging jet cell, J Appl Electrochem 27 (1997) 482–492. https://doi.org/10.1023/A:1018430224622.

[35] H. Jin, Y. Yu, L. Zhang, R. Yan, X. Chen, Polarity reversal electrochemical process for water softening, Sep Purif Technol 210 (2019) 943–949. https://doi.org/10.1016/J.SEPPUR.2018.09.009.

[36] P. V. Nidheesh, E. Mousset, A. Thiam, Recent advancements in peroxicoagulation process: An updated review, Chemosphere 339 (2023). https://doi.org/10.1016/j.chemosphere.2023.139627.

[37] P.V. Nidheesh, S.O. Ganiyu, C.A. Martínez-Huitle, E. Mousset, H. Olvera-Vargas, C. Trellu, M. Zhou, M.A. Oturan, Recent advances in electro-Fenton process and its emerging applications, Crit Rev Environ Sci Technol 53 (2023) 887–913. https://doi.org/10.1080/10643389.2022.2093074.

[38] P.V. Nidheesh, C. Trellu, H.O. Vargas, E. Mousset, S.O. Ganiyu, M.A. Oturan, Electro-Fenton process in combination with other advanced oxidation processes: Challenges and opportunities, Curr Opin Electrochem 37 (2023) 101171. https://doi.org/10.1016/j.coelec.2022.101171.

[39] F. Ferrag-Siagh, F. Fourcade, I. Soutrel, H. Aït-Amar, H. Djelal, A. Amrane, Electro-Fenton pretreatment for the improvement of tylosin biodegradability., Environ Sci Pollut Res Int 21 (2014) 8534–42. https://doi.org/10.1007/s11356-014-2771-5.

[40] F.H. Adnan, M.-N. Pons, E. Mousset, Mass transport evolution in microfluidic thin film electrochemical reactors: New correlations from millimetric to submillimetric interelectrode

distances, Electrochem Commun 130 (2021) 107097. https://doi.org/10.1016/j.elecom.2021.107097.

[41] E. Brillas, I. Sirés, M.A. Oturan, Electro-fenton process and related electrochemical technologies based on fenton's reaction chemistry, Chem Rev 109 (2009) 6570–6631. https://doi.org/10.1021/cr900136g.

[42] D. Belkheiri, Y. Kadmi, F. Fourcade, F. Geneste, D. Floner, H. AïtAmar, A. Amrane, Feasibility of combined electrochemical and biological treatment for tylosin removal, Moroccan Journal of Chemistry 2 (2014) 521–526.

[43] O. Scialdone, E. Corrado, A. Galia, I. Sirés, Electrochemical processes in macro and microfluidic cells for the abatement of chloroacetic acid from water, Electrochim Acta 132 (2014) 15–24. https://doi.org/10.1016/j.electacta.2014.03.127.

[44] J.F. Pérez, J. Llanos, C. Sáez, C. López, P. Cañizares, M.A. Rodrigo, A microfluidic flow-through electrochemical reactor for wastewater treatment: A proof-of-concept, Electrochem Commun 82 (2017) 85–88. https://doi.org/10.1016/j.elecom.2017.07.026.

[45] E. Mousset, Unprecedented reactive electro-mixing reactor: Towards synergy between micro- and macro-reactors?, Electrochem Commun 118 (2020) 106787. https://doi.org/10.1016/j.elecom.2020.106787.

[46] E. Mousset, M. Puce, M.N. Pons, Advanced Electro-Oxidation with Boron-Doped Diamond for Acetaminophen Removal from Real Wastewater in a Microfluidic Reactor: Kinetics and Mass-Transfer Studies, ChemElectroChem 6 (2019) 2908–2916. https://doi.org/10.1002/celc.201900182.

[47] O.M. Cornejo, M.F. Murrieta, L.F. Castañeda, J.L. Nava, Characterization of the reaction environment in flow reactors fitted with BDD electrodes for use in electrochemical advanced oxidation processes: A critical review, Electrochim Acta 331 (2020). https://doi.org/10.1016/j.electacta.2019.135373.

[48] Y. Lan, C. Coetsier, C. Causserand, K. Groenen Serrano, On the role of salts for the treatment of wastewaters containing pharmaceuticals by electrochemical oxidation using a boron doped diamond anode, Electrochim Acta 231 (2017) 309–318. https://doi.org/10.1016/j.electacta.2017.01.160.